buildings

MDPI

Article

Mechanical and Bond-Slip Properties of Steel-Fiber-Reinforced Geopolymer Recycled-Aggregate Concrete

Jianhua Ji [1], Zening Zhang [1], Yi Zhang [1] and Xi Liu [2,*]

[1] Northwest Engineering Corporation Limited, Xi'an 710065, China; jjianhua2025@163.com (J.J.); zzening2025@163.com (Z.Z.); zhangyi20250430@163.com (Y.Z.)
[2] School of Civil Engineering, Chang'an University, Xi'an 710064, China
* Correspondence: xliu1205@126.com

Abstract

Steel-fiber-reinforced geopolymer recycled-aggregate concrete (SFGRC) represents a promising low-carbon building material, yet data on its bond behavior remains scarce, limiting its structural application. To study the mechanical properties and bond strength of SFGRC, five groups of different mix proportions were designed. The main variation parameters were the content of recycled aggregate and the volume content of steel fiber. The cube compressive strength, splitting tensile strength, and flexural strength tests of SFGRC were completed. The influence law of different anchorage lengths on the bond strength between steel bars and SFGRC was studied through the central pull-out test. A multi-parameter probability prediction model of bond strength based on Bayesian method was established. The results show that with the increase of the content of recycled aggregate, the compressive strength of the specimen shows a downward trend, but the tension-compression ratio is increased by 18–22% compared to concrete with natural aggregates at equivalent strength grades. The content of steel fiber can significantly improve the mechanical properties of SFGRC. The bond strength between steel bars and SFGRC is 14.82–17.57 MPa, and the ultimate slip is 0.30–0.38 mm. A probability prediction model of ultimate bond strength is established based on 123 sets of bond test data. The mean and covariance of the ratio of the predicted value of the probability model to the test value are 1.14 and 2.61, respectively. The model has high prediction accuracy, and continuity and can reasonably calculate the bond strength between steel bars and SFGRC. The developed Bayesian model provides a highly accurate and reliable tool for predicting SFGRC bond strength, facilitating its safe and optimized design in sustainable construction projects.

Keywords: steel-fiber-reinforced geopolymer recycled-aggregate concrete; mechanical property; bonding strength; Bayesian; prediction model

check for updates

Academic Editor: Mijia Yang

Received: 13 May 2025
Revised: 14 June 2025
Accepted: 18 June 2025
Published: 22 June 2025

Citation: Ji, J.; Zhang, Z.; Zhang, Y.; Liu, X. Mechanical and Bond-Slip Properties of Steel-Fiber-Reinforced Geopolymer Recycled-Aggregate Concrete. *Buildings* **2025**, *15*, 2179. https://doi.org/10.3390/buildings15132179

Copyright: © 2025 by the authors. Licensee MDPI, Basel, Switzerland. This article is an open access article distributed under the terms and conditions of the Creative Commons Attribution (CC BY) license (https://creativecommons.org/licenses/by/4.0/).

1. Introduction

In the contemporary construction field, steel-fiber-reinforced geopolymer recycled-aggregate concrete (SFGRC) has emerged as a highly promising low-carbon and environmentally friendly building material, attracting increasing attention [1–3]. In terms of aggregate selection, SFGRC innovatively employs recycled aggregates to entirely replace natural coarse aggregates. This material design not only avoids the resource depletion and environmental damage caused by natural aggregate extraction but also transforms industrial waste into valuable resources, achieving efficient recycling of construction waste and aligning with the principles of green building development and circular economy

principles. Specifically, SFGRC reduces CO_2 emissions by up to 80% compared to ordinary Portland cement concrete [4–6], while recycled aggregates mitigate landfill waste and conserve natural resources.

However, the widespread adoption of geopolymer recycled-aggregate concrete and related structural components has been limited due to insufficient research data and inherent material deficiencies [7–9]. The geopolymer matrix's dense aluminosilicate gel structure offers good chemical and mechanical interlocking with steel bars. While recycled aggregates boost mechanical interlocking due to their porous nature and micro-cracks, their water absorption can affect concrete workability and bond strength. Fly ash-slag-based geopolymer concrete, owing to its favorable workability and mechanical properties, has become a focal point of research among scholars worldwide [10–13]. In addition, the microhardness of the old interfacial transition zone is approximately 41% lower than that of the new interfacial transition zone [14]. Typically, fibers are incorporated to enhance the toughness of concrete, as their physical filling and bridging effects effectively inhibit crack propagation in the geopolymer matrix, improving ductility [15,16]. Nevertheless, the performance of fiber-reinforced geopolymer concrete remains inadequately understood.

Numerous experimental studies have demonstrated that the bond strength between geopolymer concrete and steel reinforcement is generally no lower than that of ordinary cement concrete of the same strength grade, a characteristic of great significance in structural applications. Some scholars have found that the bond strength of geopolymer concrete decreases as the embedded length of the steel bar increases; the dense cementitious structure of the geopolymer endows the interface between it and the steel bar with higher bonding performance [17]. Zheng et al. [18] found that the aluminosilicate gel formed during the hydration of the geopolymer matrix possesses a denser structure compared to that of ordinary concrete. In related research, Xiao et al. [19] referenced bond-slip models for steel reinforcement in fiber-reinforced concrete and deformed bars in slag-based high-performance concrete, concluding that geopolymer recycled-concrete exhibits superior bond performance with reinforcement. Through analysis, integration, and innovation, a bond-slip relationship between deformed bars and geopolymer concrete was successfully established. However, research on the bond behavior and predictive models for SFGRC remains scarce.

In this study, SFGRC was successfully prepared. A systematic investigation was conducted to analyze how variations in steel fiber content and recycled aggregate content influence the workability and mechanical properties of SFGRC, uncovering underlying patterns to lay a theoretical foundation for future engineering applications. Additionally, central pull-out tests were performed to examine the bond behavior between SFGRC and deformed bars. Finally, 123 sets of experimental data were collected, and a bond-slip constitutive prediction model based on the Bayesian method was proposed.

2. Experimental Program

2.1. Materials

The cementitious materials used in the experiment are S95-grade slag, Class I low-calcium fly ash, and SF88-grade silica fume, and their chemical compositions are shown in Table 1.

Slag (CaO: 37.21%, Al_2O_3: 15.75%): provides calcium for rapid formation of C-A-S-H gel, accelerating early strength development, while its moderate alumina content enhances cross-linking with aluminosilicate networks. Fly ash (SiO_2: 53.26%, Al_2O_3: 33.99%): Serves as the primary aluminosilicate source, dissolving under alkali activation to form N-A-S-H geopolymer frameworks that ensure long-term durability. Its low CaO (2.46%) prevents premature setting. Silica fume (SiO_2: 90.93%): Ultra-fine particles fill nano-

pores between recycled aggregates, reducing permeability by ≈30% versus fly ash-only mixes. Its high reactivity compensates for RA's water absorption by providing additional silicates for polycondensation. This ternary system balances reaction kinetics: slag governs early strength, fly ash ensures stable geopolymer networks, and silica fume mitigates RA-induced porosity—addressing a key limitation in recycled concrete.

Table 1. Chemical composition of binders (wt%).

Material	SiO_2	Al_2O_3	Fe_2O_3	CaO	MgO	SO_3	K_2O	Na_2O
Class I Low-Calcium Fly Ash	51.494	37.186	3.515	2.793	0.414	0.831	1.109	1.145
S95-Grade Slag	32.083	15.134	0.466	38.610	8.454	2.502	0.426	0.493
SF88-Grade Silica Fume	90.442	0.805	3.555	0.632	1.044	1.336	0.949	0.292

The aggregates are recycled aggregates processed from construction demolition waste. The fineness modulus of the recycled sand is 2.23, and the particle size is ≤4.75 mm. The particle size of the coarse aggregate is ≤16 mm, and the performance indicators are shown in Table 2. Use a sodium hydroxide–sodium silicate solution with a modulus of 1.6 as the alkali activator, and select the PCA-1 type polycarboxylate superplasticizer as the admixture. The RC65/35-BN hooked-end steel fibers were selected for enhanced crack control through mechanical anchorage. Its physical properties are shown in Table 3. Select the 16 mm HRB400 steel bar. The physical property indicators are shown in Table 4.

Table 2. Physical properties of recycled aggregates.

Material	Particle Size (mm)	Bulk Density (kg/m^3)	Apparent Density (kg/m^3)	Water Absorption (%)	Crushing Index (%)
Recycled Coarse Aggregate	4.75~16.00	1250	2250	8.3	18.2
Recycled Fine Aggregate	0.15~4.75	1130	2650	11.2	14.1

Table 3. Physical properties of hooked-end steel fibers.

Fiber Type	Density (kg/m^3)	Length (mm)	Diameter (mm)	Aspect Ratio	Elastic Modulus (GPa)	Tensile Strength (MPa)
Hooked-End Steel Fiber	7800	35	0.5	65	200	1100

Table 4. Mechanical properties of steel reinforcement.

Grade	Diameter (mm)	Yield Strength (MPa)	Ultimate Strength (MPa)	Elastic Modulus (MPa)
HRB400	16	451.3	634.9	1.94 × 105

2.2. Specimen Design and Preparation

The experiment designed 5 sets of mix proportions, with the volume content of recycled aggregate being 50% and 60% and the volume content of steel fiber being 0%, 0.5%, 1%, and 1.5%. The detailed mix proportions are shown in Table 5. For each set of mix proportion, 12 cube specimens with a size of 100 mm × 100 mm × 100 mm were made, and at the same time, 3 prism specimens with a size of 100 mm × 100 mm × 400 mm were made. Under standard curing conditions, the compressive strength (f_{cu}) of the specimens

at 3 days, 7 days, and 28 days, as well as the splitting tensile strength (f_{ts}) and flexural strength (f_f) of the specimens at 28 days, were measured, respectively.

Table 5. Mix proportions of SFGRC (kg/m^3).

Mixtures	Slag	Fly Ash	Silica Fume	Recycled Fine Aggregate	Recycled Coarse Aggregate	Steel Fiber	NaOH Solution	Na_2SiO_3 Solution	Water	Water-Reducing Admixture
SFGRC-1	420	210	70	530	675	39	54	209	88	7
SFGRC-2	337	169	56	635	810	39	44	167	70	5.5
SFGRC-3	420	210	70	530	675	0	54	209	67	7
SFGRC-4	420	210	70	530	675	77	54	209	67	7
SFGRC-5	420	210	70	530	675	116	54	209	67	7

To deeply explore the bonding performance between SFGRC and steel bars, three groups of tests were designed for the SFGRC-1 mix proportion, as shown in Table 6. The focus was on the influence of the anchorage length on the bonding performance between the steel bars and concrete. The lengths of the bonding segments were set as 5d, 7.5d, and 10d, respectively. Central pull-out specimens were used, and no stirrups or transverse steel bars were set inside the specimens to ensure that the test results could accurately reflect the relationship between the anchorage length and the bonding performance. The anchoring length is located at the center of the specimen (as shown in Figure 1) to minimize the stress concentration at the end and the non-uniform bearing stress near the loading surface [20]. The cross-sections of the specimens perpendicular to the longitudinal direction of the steel bars were all 200 mm × 200 mm, and the side lengths along the longitudinal direction of the steel bars were 200 mm, 240 mm, and 280 mm, respectively. The specific structure and dimensions of the specimens are shown in Figure 1.

Table 6. Parameters and grouping of pull-out test specimens.

Mixtures	l_a/mm	l_a/d	c/mm
SFGRC-80	80	5	92
SFGRC-120	120	7.5	92
SFGRC-160	160	10	92

Notes: l_a = bond length; d = rebar diameter; and c = concrete cover thickness.

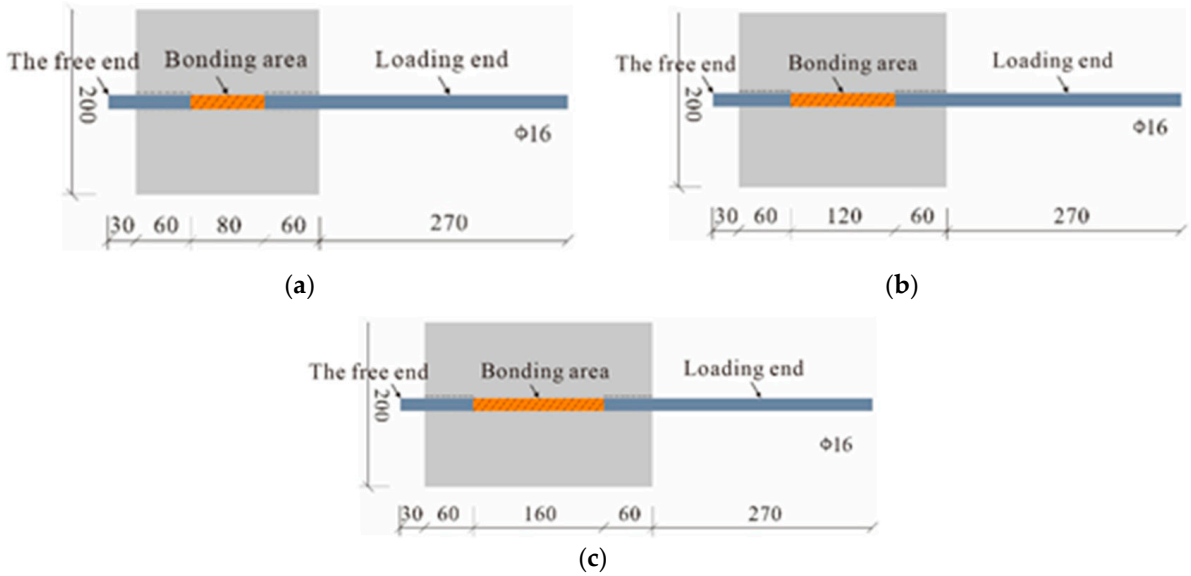


Figure 1. Schematic diagram of specimen design. (**a**) SFGRC-80. (**b**) SFGRC-120. (**c**) SFGRC-160.

2.3. Test Procedure and Loading Setup

Upon reaching the specified curing age under standard conditions, the specimens were subjected to mechanical property testing in accordance with GB/T 50081-2019 [21]. The pull-out tests were conducted using a YUL1000 electro-hydraulic servo universal testing machine (Chang'an University, Xi'an, China), with the detailed configuration of the loading setup illustrated in Figure 2. Prior to formal loading, a preload of 3 kN was applied to ensure proper contact. Displacement-controlled loading was then performed at a constant rate of 0.65 mm/min, with data acquisition at 10 Hz. Displacement transducers were installed at both the loaded and free ends of the specimens, and a DH3820 data acquisition system (Donghua Testing Technology Co., Ltd., Taizhou, China) was employed to synchronously record displacement and strain measurements. By monitoring the displacement variations on both the upper and lower surfaces of the specimens as well as at both ends of the reinforcing bar, the ultimate pull-out force was determined and the bond strength (τ_u) was subsequently calculated. The test was immediately terminated upon observation of either rebar fracture or concrete splitting failure. Post-test calculations of bond strength were performed using Equation (1) to ensure result accuracy, thereby providing reliable data for subsequent analysis.

$$\tau_u = 1000 \times \frac{F_u}{\pi d l_a} \quad (1)$$

where τ_u is the bond strength, with the unit of MPa; F_u is the maximum load at failure, with the unit of kN; d is the diameter of the steel bar, with the unit of mm; and l_a s the bond and anchorage length of the steel bar, with the unit of mm.

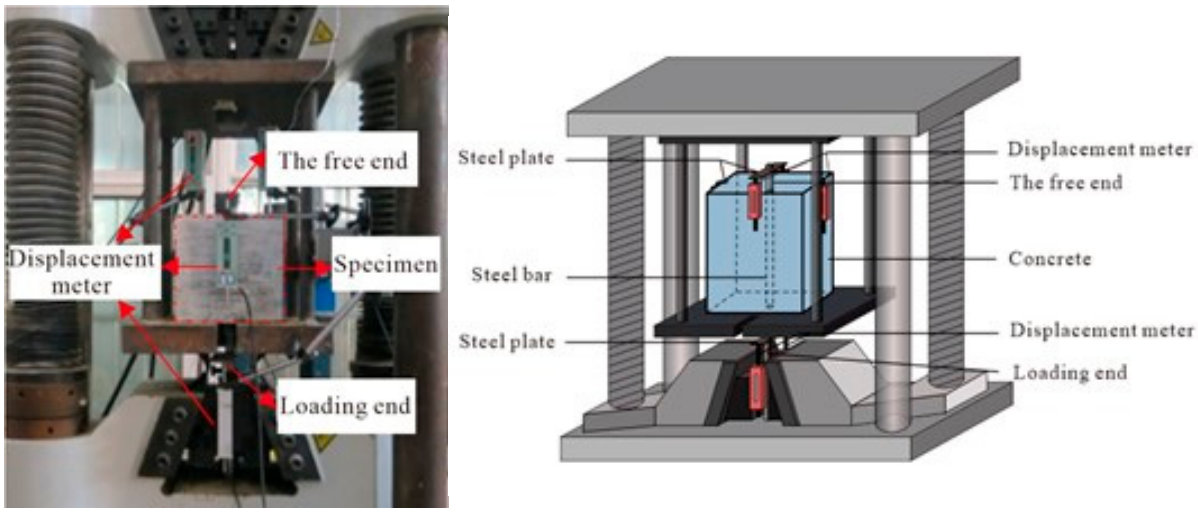


Figure 2. Loading setup diagram.

3. Results and Analysis

3.1. Workability

Table 7 presents the experimental results of the physical and mechanical properties of geopolymer recycled-aggregate concrete. As shown, the 28-day oven-dry density of SFGRC ranged from 1856 kg/m^3 to 2004 kg/m^3, which is lower than that of conventional concrete. This reduction is primarily attributed to the incorporation of low-density recycled aggregates that decreased the overall concrete density.

The slump values of SFGRC varied between 121 mm and 177 mm across different mix proportions. According to the Standard for Quality Control of Concrete (GB 50164-2011) [22], all prepared SFGRC mixtures met the engineering requirements. Experimental findings revealed that increasing the content of recycled aggregates and steel

fibers significantly reduced the workability of concrete. This phenomenon can be explained by two main factors: First, the recycled aggregate has a relatively strong water absorption, which reduces the effective water content in the mixture and increases the internal friction. Second, the steel fibers form a spatial network structure in the mixture, which restricts and hinders the flow of the mixture, ultimately leading to a decrease in slump.

Table 7. Fundamental properties of SFGRC.

Mixtures	Slump (mm)	ρ_d /(kg/m^3)	$f_{cu,3d}$ /MPa	$f_{cu,7d}$ /MPa	$f_{cu,28d}$ /MPa	f_{ts} /MPa	f_f /MPa
SFGRC-1	156	1947	28.18	32.08	43.13	3.27	3.77
SFGRC-2	146	1889	20.69	26.39	25.23	2.35	2.62
SFGRC-3	177	1856	24.82	31.10	34.57	1.82	2.92
SFGRC-4	137	1959	26.06	30.15	39.83	4.28	4.80
SFGRC-5	121	2004	27.98	33.54	40.10	4.71	5.93

Note: ρ_d: dry apparent density; f_{cu}: cube compressive strength; f_{ts}: splitting tensile strength; and f_f: flexural strength.

3.2. Compressive Strength

Figure 3 clearly illustrates the early-age strength development characteristics of SFGRC under different mix proportions. The experimental results demonstrate that the 3-day compressive strength reaches 65–76% of the 28-day strength, while the 7-day strength attains 77–96% of the ultimate strength. This significantly outperforms conventional OPC concrete, where typical 3-day and 7-day strengths are only 25–40% and 60–75% of the 28-day strength, respectively, for equivalent C30–C50 grades. The accelerated strength gain stems from geopolymerization kinetics—slag dissolution releases Ca^{2+} ions within 24 h, forming C-A-S-H gels 3× faster than OPC hydration—enabling formwork removal 40% earlier than OPC systems in practice. The 41.5% reduction in compressive strength when recycled aggregate content increased from 50% to 60% stems from three microstructural limitations. This reduction primarily stems from inherent defects in recycled aggregates, including microcracks, high porosity, and multiple weak interfacial transition zones (ITZs), which promote stress concentration under loading.

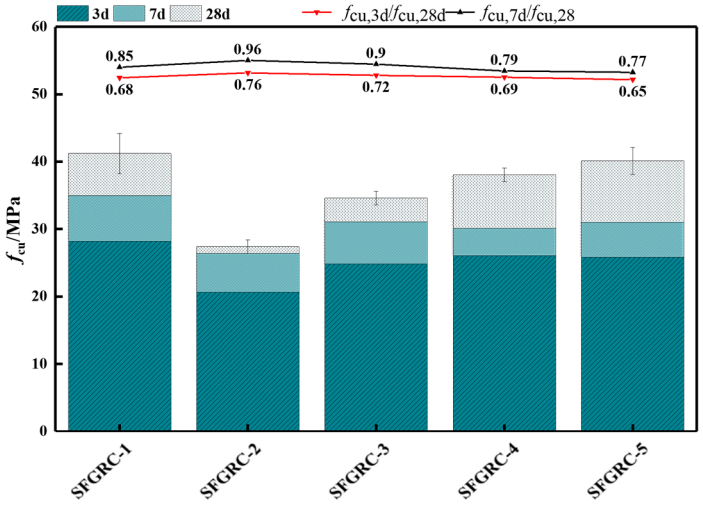


Figure 3. Cubic compressive strength of SFGRC.

Regarding the effect of steel fiber content, the compressive strength of SFGRC exhibited a progressive increase from 34.57 MPa to 43.13 MPa as the fiber volume fraction rose from 0% to 0.50%. However, further fiber addition beyond 0.5% resulted in a 24.76% strength

reduction compared to the optimal fiber content. This phenomenon is attributed to fiber clustering and overlapping at higher dosages, which entraps air voids and compromises material compactness, ultimately impairing mechanical performance.

3.3. Splitting Tensile and Flexural Strength

Figure 4 shows the splitting tensile strength and flexural strength of SFGRC with different proportions. It has been determined that the tensile-compressive ratio of SFGRC is in the range of 0.053 to 0.125, and this value is basically the same as that of ordinary concrete. Through a direct observation of the failure surface of the splitting tensile test block (as shown in Figure 5), it can be clearly seen that when the geopolymer recycled-concrete fails, its cracks exhibit the characteristic of crossing through the coarse aggregate. This is mainly due to the low strength of the recycled aggregate itself, as well as the presence of a large number of pores inside and a relatively weak interfacial transition zone. When the volume content of the recycled aggregate increases from 50% to 60%, the flexural strength and splitting tensile strength decrease from 3.27 MPa and 3.77 MPa to 2.35 MPa and 2.62 MPa, respectively. As the content of steel fibers increases from 0 to 0.5%, 1%, and 1.5%, the splitting tensile strength and flexural strength increase by 10.99% to 158.79% and 36.97% to 113.80%, respectively, and the tensile-compressive ratio and flexural-compressive ratio increase from 5.31% and 8.51% to 7.6% to 11.4% and 8.74% to 14.39%, respectively. This strengthening effect is mainly derived from the bridging effect of the steel fibers between the matrix and the aggregate, and the mechanical interlocking and cementation between the steel fibers and the matrix significantly improve the tensile, flexural properties, and toughness of the material.

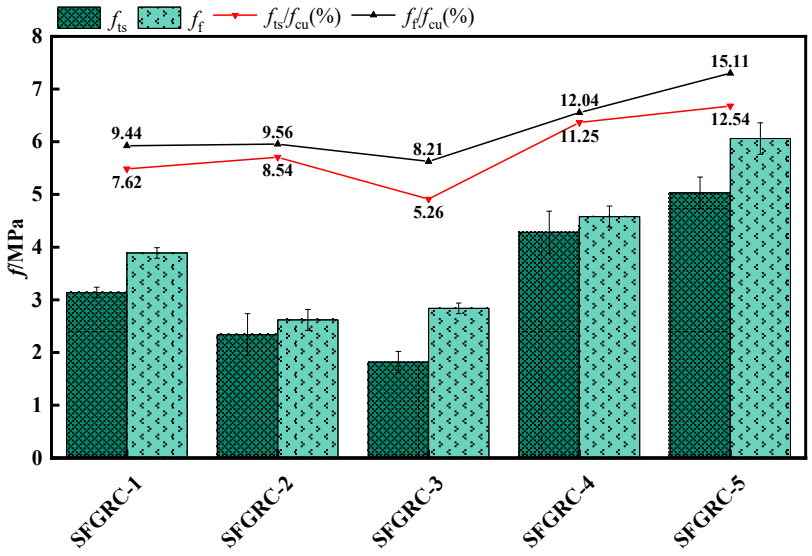
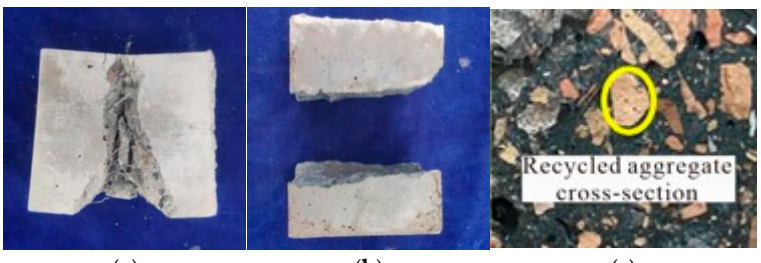


Figure 4. Splitting tensile strength and flexural strength of SFGRC.



(**a**) (**b**) (**c**)

Figure 5. Fracture surface of splitting tensile specimen. (**a**) SFGRC-1. (**b**) SFGRC-3. (**c**) concrete section.

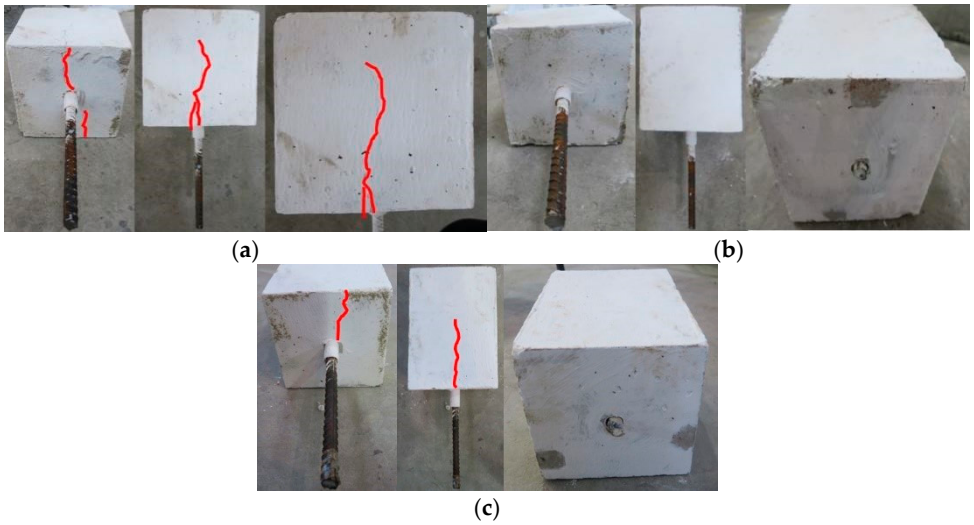
3.4. Bond-Slip

3.4.1. Failure Modes

In the pull-out test, there are usually three typical failure modes: concrete splitting, steel bar pulling out, and splitting-pulling out composite failure. All the specimens in the test exhibited the failure mode of steel bar pulling out. All the specimens failed due to the cracking of the concrete in the bonding area between the steel bar and the concrete.

At the initial stage of loading, there was no obvious change on the surface of the concrete. The tensioned steel bar only produced elastic deformation, and there was no relative slip phenomenon at the free end of the steel bar. As the load continued to increase steadily, the slip amount between the steel bar and the concrete interface began to gradually rise. When the load reached the limit value, a slight cracking sound could be heard from inside the concrete. At the same time, the load value began to show a downward trend. As the load continued to increase, the relative slip amount between the free end of the steel bar and the concrete continued to accumulate. When the relative slip amount reached 10 mm, the stress state of the specimen changed significantly and entered a stable residual slip stage. In this stage, although the specimen still maintained a certain structural form, its bearing capacity had been greatly reduced.

With the passage of time and the continuous action of the load, the bonding force inside the specimen was completely destroyed, and finally the steel bar pulling out failure occurred, leading to the failure of the entire specimen. The failure mode of the specimen is shown in Figure 6.



(**a**) (**b**) (**c**)

Figure 6. Failure modes of specimens. (**a**) SFGRC-80. (**b**) SFGRC-120. (**c**) SFGRC-160.

3.4.2. Bond-Slip Curves

The test results of the bonding performance between the steel bars and SFGRC are shown in Figure 7 and Table 8; it can be seen that there is an inverse correlation between the bonding strength of the specimens and the length of the anchorage section. Through the analysis of the test data, there is a significant negative correlation between the length of the anchorage section and the bonding strength. As the length of the anchorage section gradually increases, the bonding strength shows a continuous decreasing trend.

Taking the specimen with a bonding length of 5d as the reference benchmark, when the bonding length increases to 10d, the bonding strength of the specimen decreases by 11.3%. When the bonding length is 7.5d, the decrease in the bonding strength of the specimen is more significant, reaching 15.65%, and the ultimate slip decreases by 10.5% and 21.0%, respectively. This is because of the differences in the material properties of the

concrete itself; the unevenness of the interfacial microstructure between the steel bar and the concrete; and possible insufficient vibration during the construction process, etc., which lead to the uneven distribution of the bonding stress of the steel bar inside the concrete. The tensile stress of the steel bar decays rapidly from the loading end to the free end. This phenomenon greatly affects the cooperative working performance between the steel bar and the concrete, and thus leading to a downward trend in the average bonding strength.

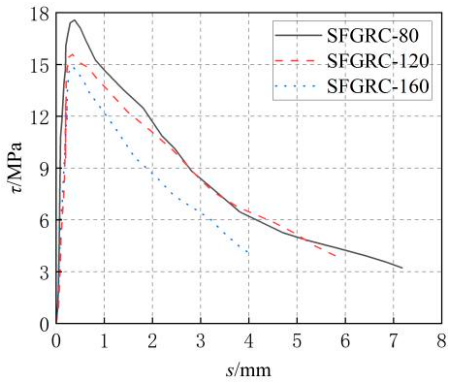


Figure 7. Bond-slip curve of the specimen.

Table 8. Bond-slip test results.

Mixtures	Ultimate Load F_u/kN	Ultimate Bond Strength τ_u/MPa	Ultimate Slip s_u/mm	Steel Stress τ_s/MPa	Failure Mode
SFGRC-80-2	70.61	17.57	0.38	348.07	Pull-out
SFGRC-120-2	93.93	15.58	0.34	484.17	Pull-out after yielding
SFGRC-160-2	119.13	14.82	0.30	595.69	Pull-out after yielding

4. Bayesian Theory-Based Prediction Model for Bond Strength of SFGRC

4.1. Bayesian Method

Using established design calculation methods and experimental data as prior information, the Bayesian hypothesis is selected as the prior distribution. Under this premise, the Bayesian probabilistic statistical method is employed to comprehensively integrate and rigorously infer the two types of prior information—design calculation methods and experimental data. The specific model is presented in Equation (2):

$$F(X,\Theta) = F_{\mathrm{d}}(X) + \sum_{i=1}^{p} \theta_i h_i(x) + \sigma\varepsilon \tag{2}$$

where X represents the vector form of influencing factors; $\Theta = (\theta, \sigma)$ denotes the unknown model parameters, which can be estimated using the Bayesian method combined with experimental data; $F_{\mathrm{d}}(X)$ is the existing bond strength calculation model; $\sum_{i=1}^{p} \theta_i h_i(x)$ is the corresponding correction term, expressed as a function of parameter X and the unknown model parameters $\theta = [\theta_1, \theta_2, \ldots, \theta_{\mathrm{p}}]^{\mathrm{T}}$; ε is a normally distributed random variable, satisfying $\varepsilon \sim N(0, 1)$; and σ represents the residual error remaining after model correction. $h_i(x)$ is a function selected based on mechanical theory or existing research findings, used to evaluate the influence parameters. Perform a logarithmic operation on Equation (3) in the following form:

$$\ln[F(X,\Theta)] = \ln[F_d(X)] + \sum_{i=1}^{p} \theta_i h_i(x) + \sigma\varepsilon \tag{3}$$

4.2. Database

This study comprehensively collected 123 sets of experimental data on the bond behavior between steel reinforcement and geopolymer recycled-aggregate concrete, covering both beam-type and central pull-out specimens. Key parameters are concrete compressive strength (f_{cu}), cover thickness (c), water-to-binder ratio (w/b), anchorage length (l), reinforcement diameter (d), stirrup reinforcement ratio (ρ), recycled aggregate replacement ratio, and fiber content. All data were systematically compiled and are clearly presented in Table 9.

Table 9. Summary of bond anchorage test data.

Reference	Number	Compressive Strength f_{cu}/MPa	Cover Thickness c/d	Anchorage Length l/mm	Rebar Diameter d/mm	Recycled Aggregate Replacement Ratio R	Fiber Content F	τ_u /MPa
Zheng Yongqian [18]	51	20.6~78.8	2.63~5.75	1d~8d	12~22	0~100	0	10.45~32.54
Zhang Haiyan [23]	8	45.3~48.1	8.6	5d~12d	16	0	0	9.8~23.9
Li Guanghui [24]	9	24.6~41.8	8.3	3.5d	6	0	0	0.72~4.29
Xiao Jianzhuang [18]	17	36.1~48.1	2.27~7.0	5d~9d	10~25	0	0	10.91~19.71
Seshu [25]	20	26~61.2	4.19	2d~5d	16	0~100	0	13.53~30.13
Abdulrahman [26]	9	24~43.2	2.6~4.5	5d	10~16	0	0	9.9~22.1
Le [27]	9	20.3~41.1	1.19~5.75	5d~8.33d	12~20	0	0	6.01~15.4
Yang [28]	20	32.5~154.5	1.61~8.875	3d	8~14	0	2.5%	4.75~35.44

4.3. Probabilistic Model Development

To achieve more precise analysis and uncover the underlying patterns in the data, this study integrates Bayesian methods with 123 sets of experimental data. The research thoroughly accounts for various potential sources of uncertainty, such as subtle environmental variations and fluctuations in material properties. Leveraging the robust data processing and statistical analysis capabilities of R (v4.5.1—https://www.r-project.org/, accessed on 17 June 2025), a meticulously crafted script was developed to enable in-depth data mining and effective analysis. The iterative parameter results were then substituted into Equation (4) for exponential computation. Using Bayesian parameter elimination, parameters with negligible influence on bond strength were progressively removed, ultimately establishing a multi-parameter probabilistic model for bond strength.

$$\tau_{u.B} = 4.981 \cdot {f_{cu}}^{0.543} \cdot \left(\frac{l}{d}\right)^{-0.754} \cdot \left(\frac{c}{d}\right)^{0.642} \cdot e^{(1.021\rho_{sv}+0.895R+0.796F)}. \quad (4)$$

where $\tau_{u,B}$ represents bond strength; f_{cu} represents cubic compressive strength; l represents bonding length; d represents steel bar diameter; and c represents cover thickness.

4.4. Model Validation

To account for various influencing factors, scholars have proposed multiple models for calculating the ultimate bond strength, including classical models by Xu Youlin [29], GB 50010-2010 [30], Ye Lieping [31], and Tepfers [32].

Table 10 and Figure 8 visually present the distribution of the ratio between the experimental and predicted results for each model. A comparative analysis reveals that the probabilistic model exhibits a mean value of 1.14 and a coefficient of variation (CoV) of 2.61, indicating relatively small deviations. Specifically, both the mean and median values are close to 1, with low dispersion and fewer outliers generated during computation. In contrast, the GB 50010-2010 [30] and Tepfers [32] models, due to their limited consideration of influencing factors, demonstrate inferior prediction accuracy and higher variability.

The results further confirm that the Bayesian method effectively identifies key factors significantly affecting bond strength.

Table 10. Calculation results of various models.

Model	Calculation Formula	Mean	SD	CoV	R^2
Probabilistic model	$\tau_{u.B} = 4.981 \cdot {f_{cu}}^{0.543} \cdot \left(\frac{l}{d}\right)^{-0.754} \cdot \left(\frac{c}{d}\right)^{0.642} \cdot e^{(1.021\rho_{sv}+0.895R+0.796F)}$	1.14	2.98	2.61	0.89
Xu [29]	$\tau_u = (1.6 + 0.7\frac{c}{d} + 20\rho_{sv})f_t$	1.96	10.25	5.23	0.81
GB50010-2010 [30]	$\tau_u = 3f_{t,r}$	0.95	6.50	6.63	0.73
Ye [31]	$\tau_u = (0.3 + 3.5\frac{d}{l})(3.5 + 0.45\frac{c}{d} + 4.1\sqrt{\rho_{sv}})f_{cu}^{0.55}$	5.36	32.09	5.98	0.42
Tepfers [32]	$\tau_u = (\frac{c+d/2}{1.664d})f_t$	1.33	9.11	6.84	0.67

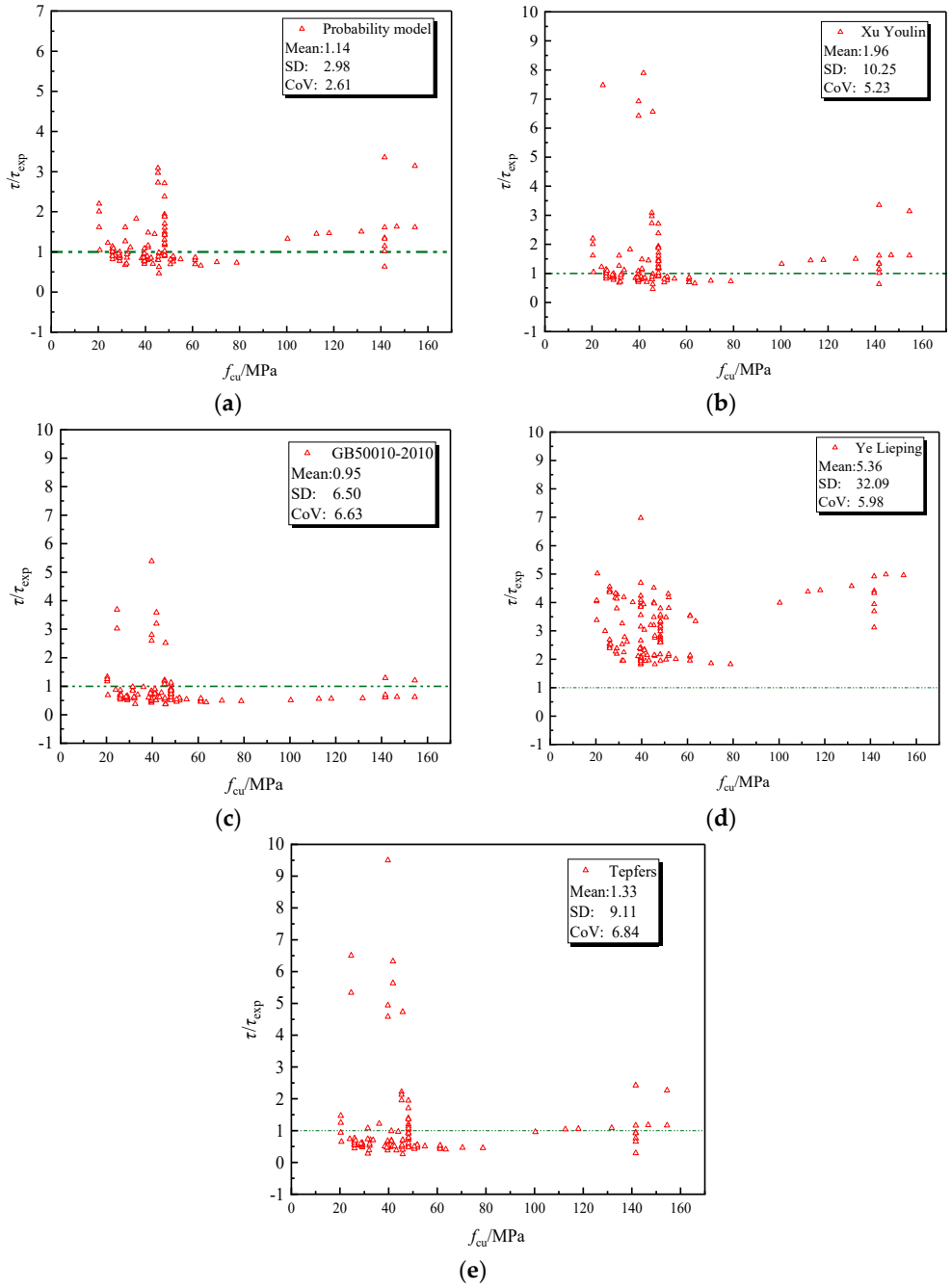


Figure 8. Error analysis of model predictions. (**a**) Probabilistic model. (**b**) Xu Youlin [29]. (**c**) GB 50010-2010 [30]. (**d**) Ye Lieping [31]. (**e**) Tepfers [32].

5. Conclusions

This paper designs five groups of different mix proportions to study the mechanical properties and bond strength of steel-fiber geopolymer recycled-concrete. Compared with fiber-reinforced ordinary Portland cement (OPC) concrete and ordinary geopolymer concrete, steel-fiber geopolymer recycled-concrete (SFGRC) has higher mechanical efficiency and stronger bond performance. The unique combination of geopolymer binder, recycled aggregates, and steel fibers produces a synergistic effect, making SFGRC a promising material for sustainable infrastructure. The main research conclusions are as follows:

(1) The dry apparent density of steel-fiber geopolymer recycled-aggregate concrete (SFGRC) ranges from 1856 kg/m^3 to 2004 kg/m^3. The slump value of the concrete is between 121 and 177 mm, and its fluidity decreases with the increase in the amount of recycled aggregate and steel fiber.

(2) As the content of recycled aggregates increases, the compressive strength of SFGRC decreases by 41.5%, but the tensile-compressive ratio increases by 18–22%. When the volume fraction of steel fibers increases from 0% to 1.5%, the splitting tensile strength increases by 10.99–158.79%, and the flexural strength increases by 36.97–113.80%. The dry apparent density of the material is 10–15% lower than that of traditional concrete, but the workability decreases with the increase of recycled aggregates and fiber content.

(3) The bond strength between the SFGRC and steel bars is 14.82–17.57 MPa. When the anchorage length increases from 5d to 10d, the bond strength decreases by 11.3%, and the ultimate slip amount is 0.30–0.38 mm. The failure mode is dominated by steel bar pull-out. The porous structure of recycled aggregates improves the bond strength through the mechanical interlocking effect, but an excessively long anchorage length will lead to non-uniform stress distribution.

(4) Based on 123 sets of test data, a Bayesian probability model is established. The predicted mean ratio of bond strength is 1.14, and the coefficient of variation is 2.61. It is verified that the model can accurately predict the bond strength of SFGRC, providing strong theoretical support and data reference for subsequent engineering applications and further research.

These findings collectively advance sustainable construction by transforming waste streams into high-performance structural materials while providing the predictive rigor demanded by engineering practice.

Author Contributions: Conceptualization, J.J., Y.Z. and X.L.; methodology, J.J., Z.Z. and Y.Z.; software, Z.Z. and X.L.; formal analysis, J.J., Z.Z. and Y.Z.; investigation, J.J. and Y.Z.; resources, Z.Z. and X.L.; writing—original draft preparation, J.J.; writing—review and editing, Z.Z., Y.Z. and X.L.; and funding acquisition, J.J. All authors have read and agreed to the published version of the manuscript.

Funding: This research was funded by the National Natural Science Foundation of China, China (52478297); the Key Research and Development Program of Shaanxi Province, China (2024SF-YBXM-609, 2024GX-YBXM-177); and the Scientific Research Plan Projects of Shaanxi Education Department, China (23JE004).

Data Availability Statement: Data is contained within the article.

Conflicts of Interest: Authors Jianhua Ji, Zening Zhang and Yi Zhang were employed by the company Northwest Engineering Corporation Limited. The remaining authors declare that the research was conducted in the absence of any commercial or financial relationships that could be construed as a potential conflict of interest.

References

1. Sabau, M.; Bompa, D.; Silva, L. Comparative carbon emission assessments of recycled and natural aggregate concrete: Environmental influence of cement content. *Geosci. Front.* **2021**, *12*, 101235. [CrossRef]
2. Global Alliance for Buildings and Construction. *Global Status Report for Buildings and Construction*; United Nations Environment Programme: New York, NY, USA, 2025.
3. Zhang, B.; Feng, Y.; Xie, J.; Dai, J.; Chen, W.; Xue, Z.; Li, L.; Li, Y.; Li, J. Effects of pretreated recycled powder substitution on mechanical properties and microstructures of alkali-activated cement. *Constr. Build. Mater.* **2023**, *406*, 133360. [CrossRef]
4. McLellan, B.C.; Williams, R.P.; Lay, J.; van Riessen, A.; Corder, G.D. Costs and carbon emissions for geopolymer pastes in comparison to ordinary portland cement. *J. Clean. Prod.* **2011**, *19*, 1080–1090. [CrossRef]
5. Zhang, B.; Liu, Y.; Pan, Z.; Li, L.; Huang, Y.; Wang, Z.; Chen, J.; Lao, W.; Liu, F.; Zhu, H.; et al. The microstructure and mechanical properties of recycled metakaolinite-based geopolymer: Dependence of recycled powder replacement ratio. *J. Build. Eng.* **2024**, *85*, 108730. [CrossRef]
6. Ma, Z.; Wu, Y.; Yang, D.; Fang, K.; Hou, S.; Dai, Y.; Wang, C. Upcycling of recycled brick powder as a substitute for precursor and sand in completely recycled geopolymer: From micro to macro perspective. *Constr. Build. Mater.* **2025**, *476*, 141300. [CrossRef]
7. Teh, S.H.; Wiedmann, T.; Castel, A.; de Burgh, J. Hybrid life cycle assessment of greenhouse gas emissions from cement, concrete and geopolymer concrete in Australia. *J. Clean. Prod.* **2017**, *152*, 312–320. [CrossRef]
8. Asadollahfardi, G.; Katebi, A.; Taherian, P.; Panahandeh, A. Environmental life cycle assessment of concrete with different mixed designs. *Int. J. Constr. Manag.* **2021**, *21*, 665–676. [CrossRef]
9. Hu, Y.; Tang, Z.; Li, W.; Li, Y.; Tam, V.W.Y. Physical-mechanical properties of fly ash/GGBFS geopolymer composites with recycled aggregates. *Constr. Build. Mater.* **2019**, *226*, 139–151. [CrossRef]
10. Singh, B.; Ishwarya, G.; Gupta, M.; Bhattacharyya, S. Geopolymer concrete: A review of some recent developments. *Constr. Build. Mater.* **2015**, *85*, 78–90. [CrossRef]
11. Zhang, P.; Gao, Z.; Wang, J.; Guo, J.; Hu, S.; Ling, Y. Properties of fresh and hardened fly ash/slag based geopolymer concrete: A review. *J. Clean. Prod.* **2020**, *270*, 122389. [CrossRef]
12. Winnefeld, F.; Leemann, A.; Lucuk, M.; Svoboda, P.; Neuroth, M. Assessment of phase formation in alkali activated low and high calcium fly ashes in building materials. *Constr. Build. Mater.* **2010**, *24*, 1086–1093. [CrossRef]
13. Wijayasundara, M.; Crawford, R.H.; Mendis, P. Comparative assessment of embodied energy of recycled aggregate concrete. *J. Clean. Prod.* **2017**, *152*, 406–419. [CrossRef]
14. Shilar, F.A.; Ganachari, S.V.; Patil, V.B.; Khan, T.M.Y.; Javed, S.; Baig, R.U. Optimization of Alkaline Activator on the Strength Properties of Geopolymer Concrete. *Polymers* **2022**, *14*, 2434. [CrossRef]
15. Farhan, N.A.; Sheikh, M.N.; Hadi, M.N.S. Effect of Steel Fiber on Engineering Properties of Geopolymer Concrete. *Mater. J.* **2020**, *117*, 29–40.
16. Wen, Y.; Liu, X.; Sun, G.Y.; Shen, W.S. Mechanical properties and stress-strain relationship of steel fiber reinforced geopolymer recycled concrete. *Structures* **2025**, *75*, 108697. [CrossRef]
17. Wang, H.L.; Sun, X.Y.; Peng, G.Y. Experimental study on bond behaviour between BFRP bar and engineered cementitious composite. *Constr. Build. Mater.* **2015**, *95*, 448–456. [CrossRef]
18. Zheng, Y.; Xiao, Y. A comparative study on strength, bond-slip performance, and microstructure of geopolymer/ordinary recycled brick aggregate concrete. *Constr. Build. Mater.* **2023**, *366*, 130257. [CrossRef]
19. Xiao, J.; Xie, M.; Zhang, C. Residual compressive behavior of pre-heated high-performance concrete with blast-furnace-slag. *Fire Saf. J.* **2006**, *41*, 91–98. [CrossRef]
20. Darwin, D.; Graham, E.K. Effect of Deformation Height and Spacing on Bond Strength of Reinforcing Bars. *ACI Struct. J.* **1993**, *90*, 646–657.
21. *GB/T 50081-2019*; Standard for Test Methods of Physical and Mechanical Properties of Concrete. China Architecture & Building Press: Beijing, China, 2018.
22. *GB 50164-2011*; Standard for Quality Control of Concrete. China Architecture & Building Press: Beijing, China, 2010.
23. Zhang, H.; Li, Q.; Jiang, W.; Quan, J. Bond anchorage performance of geopolymer mortar planted bars. *J. South China Univ. Technol.* **2021**, *49*, 65–74+84. (In Chinese)
24. Li, G.; Wang, Z.; Pan, H.; Yang, S.; Yang, Y. Experimental study on bond behavior between CFRP/steel bars and new concrete. *Concrete* **2023**, *7*, 28–33+38. (In Chinese)
25. Seshu, D.R. A Comparative Study on Bond Strength of Normal and Geopolymer Concrete to Steel Bar. Cement Wapno Beton. 2004. Available online: https://www.cementwapnobeton.pl/pdf-176667-97397?filename=A%20comparative%20study%20on.pdf (accessed on 17 June 2025).
26. Abdulrahman, H.; Muhamad, R.; Visintin, P.; Shukri, A.A. Mechanical properties and bond stress-slip behaviour of fly ash geopolymer concrete. *Constr. Build. Mater.* **2022**, *327*, 126909. [CrossRef]

27. Le, T.A.; Nguyen, T.N.; Nguyen, K.T. Experimental, Numerical, and Theoretical Studies of Bond Behavior of Reinforced Fly Ash-Based Geopolymer Concrete. *Appl. Sci.* **2022**, *12*, 7812. [CrossRef]
28. Yang, T.; Xu, S.; Liu, Z.; Li, J.; Wu, P.; Yang, Y.; Wu, C. Experimental and numerical investigation of bond behavior between geopolymer based ultra-high-performance concrete and steel bars. *Constr. Build. Mater.* **2022**, *345*, 128220. [CrossRef]
29. Xu, Y.L. Simplified model for bond-slip constitutive relationship between steel bars and concrete. *Eng. Mech.* **1997**, *2*, 34–38. (In Chinese)
30. *GB 50010-2010*; Code for Design of Concrete Structures. China Architecture & Building Press: Beijing, China, 2010.
31. Li, Y.J.; Ye, L.P.; Cheng, Z.J.; Wang, X.F.; Ding, J.T. Experimental study on bond anchorage strength between high-strength ceramsite concrete and deformed bars. *Build. Sci.* **2006**, *4*, 51–55. (In Chinese)
32. Tepfers, R. Cracking of concrete cover along anchored deformed reinforcing bars. *Mag. Concr. Res.* **1979**, *31*, 3–12. [CrossRef]

Disclaimer/Publisher's Note: The statements, opinions and data contained in all publications are solely those of the individual author(s) and contributor(s) and not of MDPI and/or the editor(s). MDPI and/or the editor(s) disclaim responsibility for any injury to people or property resulting from any ideas, methods, instructions or products referred to in the content.